Tuning the Two-Dimensional Electron Gas at Oxide Interfaces with Ti-O Configurations: Evidence from X-ray Photoelectron Spectroscopy

Zhang, Yu ; Gan, Yulin; Niu, Wei ; Norrman, Kion; Yan, Xi ; Christensen, Dennis Valbjørn; von Soosten, Merlin; Zhang, Hongrui ; Shen, Baogen; Pryds, Nini

Total number of authors:
12

Published in:
A C S Applied Materials and Interfaces

Link to article, DOI:
10.1021/acsami.7b16510

Publication date:
2018

Document Version
Peer reviewed version

Tuning the Two-Dimensional Electron Gas at Oxide Interfaces with Ti-O Configurations: Evidence from X-ray Photoelectron Spectroscopy

Yu Zhang[1,2], Yulin Gan[2], Wei Niu[2], Kion Norrman[2], Xi Yan[1], Dennis Valbjørn Christensen[2], Merlin von Soosten[2], Hongrui Zhang[1], Baogen Shen[1], Nini Pryds[2], Jirong Sun[1] and Yunzhong Chen[2*]*

[1]Beijing National Laboratory for Condensed Matter Physics and Institute of Physics, Chinese Academy of Sciences, Beijing 100190, Peoples' Republic of China

School of Physical Sciences, University of Chinese Academy of Sciences, Beijing 100049, Peoples' Republic of China

[2]Department of Energy Conversion and Storage, Technical University of Denmark, Risø Campus, 4000 Roskilde, Denmark

KEYWORDS: two-dimensional electron gas, redox reaction, TiO_2, $SrTiO_3$, oxygen vacancies.

ABSTRACT: Chemical redox reaction can lead to a two-dimensional electron gas (2DEG) at the interface between a TiO_2-terminated $SrTiO_3$ (STO) substrate and an amorphous $LaAlO_3$ (a-LAO) capping layer. When replacing the STO substrate with rutile and anatase TiO_2 substrates, considerable differences in interfacial conduction are observed. Based on X-ray photoelectron spectroscopy (XPS) and transport measurements, we conclude that the interfacial conduction comes from redox reactions,

and that the differences among the materials systems result mainly from variations in the activation energies for the diffusion of oxygen vacancies at substrate surfaces.

1. INTRODUCTION

As silicon is the foundation material for semiconductor technology, strontium titanate, $SrTiO_3$ (STO), is the base material for the emerging field of oxide electronics. Two-dimensional electron gases (2DEGs) at STO-based heterointerfaces,[1-4] $LaAlO_3/SrTiO_3$ (LAO/STO) in particular,[1] exhibit a large number of remarkable physical properties, such as superconductivity,[5] magnetism,[6] sensitivity to electric field,[7] light illumination,[8] and high electron mobility,[9-10] which show potential applications in the next generation of electronic devices.[11] Despite intensive research, the origin of the conductivity at the LAO/STO interface remains hotly debated.[12-17] Different scenarios have been proposed, including the charge transfer from LAO surface to interface due to polar discontinuity,[1, 12] extrinsic doping by generation of oxygen vacancies in STO substrate,[4, 13-15] and extrinsic doping by cation intermixing across the interface to induce *n*-type conduction of La-doped STO.[16] Among these, formation of oxygen vacancies into STO substrate frequently occurs while depositing oxide capping layers[18-24] that contain specific active elements, such as Al, Hf, Zr and Ti on the top of STO. During the deposition process, oxygen ions in the STO substrate will diffuse outward to oxidize the reactive plasma species absorbed on the substrate surface, leaving behind oxygen vacancies in the STO substrate.[18] This in turn gives rise to a 2DEG confined to the interface as what occurred for the amorphous-$LaAlO_3$ (a-LAO)/STO interface grown at room temperature.[18] Using O^{18}-exchanged STO substrates, the significant oxygen transfer from substrate to the film has been experimentally observed for both high temperature and room temperature film deposition using pulsed laser deposition (PLD).[25-26] Agham *et*

al[21] also reported that when metals were deposited on the STO substrate, an oxygen-deficient layer in STO is very likely to be created if the formation energy of the metal oxide is larger than that of an oxygen vacancy. So far, generating oxide 2DEGs by redox reactions has been largely limited to the STO substrate, for which various capping layers have been adopted, such as a-LAO,[22] amorphous $CaHfO_3$,[20] yttria-stabilized zirconia (YSZ),[18] and Al_2O_3.[4, 19] Besides (001)-oriented STO substrates, STO with orientations of (110) and (111)[27] has also been used for the deposition of a-LAO. Recently, Sarkar *et al*[28] replaced the STO substrate of a-LAO/STO heterostructures with anatase TiO_2 [TiO_2(A)] and rutile TiO_2 [TiO_2(R)] and obtained interfacial 2DEGs with different transport properties from a-LAO/STO. However, the origin underlying the transport differences remains open. Herein, we employed both transport and X-ray photoelectron spectroscopy (XPS) measurements to study the formation of 2DEGs between a-LAO and STO, TiO_2(A) or TiO_2(R) with different Ti-O-Ti bond configurations. Similar to previous reports, we found that the a-LAO/STO interface is metallic from 295 K to 2 K with a typical carrier density of 1.0×10^{14} cm^{-2} at 295 K. The a-LAO/TiO_2(A) interface shows a similar metallic behavior to a-LAO/STO except for a resistance upturn below 125 K, which is likely to be due to the Kondo effect. Moreover, the a-LAO/TiO_2(R) interface exhibits a carrier density lower by a factor of 18 than the former two systems and displays a metal-to-insulator transition at 45 K upon cooling. Our XPS measurements indicate that the differences in transport properties of these three heterostructures is ascribed mainly to the different activation energies for the diffusion of oxygen vacancies from the substrate to the a-LAO capping layer during the interfacial redox reactions.

2. EXPERIMENTAL DETAILS

Three types of substrates were employed, STO (001), TiO_2(A) (001) and TiO_2(R) (001) with a size of $5\times5\times0.5$ mm^3. The TiO_2(R) and STO are commercial substrates. To get a TiO_2-terminated layer,

the STO substrate was chemically etched by a HCl-HNO_3 acidic solution, and then annealed at 1000 ºC for 1 h in 1 bar oxygen. The crystalline TiO_2(A) substrate was grown by PLD (KrF excimer laser, λ=248 nm) on the LAO substrate at 750°C under an oxygen pressure of 5×10^{-3} mbar. The films obtained (about 100 nm) are confirmed to be of high crystalline quality by X-ray diffraction (XRD), with a smooth surface (root mean square roughness is 1.1 nm, Supporting Information S1). The heterostructures were formed by capping the three substrates with a-LAO films grown by PLD with a commercial LAO single crystal target. This amorphous capping layer is nonpolar therefore rules out the polar discontinuity induced electronic reconstruction in the all-crystalline heterointerface.[1,29] During the deposition, the substrate was kept at room temperature and the oxygen pressure was maintained to 10^{-6} mbar. The laser fluence is 3 Jcm^{-2} and the repetition rate is 1 Hz. The target-substrate distance was fixed at 5 cm. The thickness of the a-LAO capping layer was kept at 3 nm in this work. However, samples with the a-LAO films up to the thickness of 16 nm showed similar results (Supporting Information S4).

Transport measurements were done in both van der Pauw and Hall-bar geometry with the latter prepared by depositing a-LAO through a mechanical mask. Ultrasonic Al wire bonding was used to get electric connection. The electric measurements were performed in a CRYOGENIC cryogen-free measurement system in the temperature range from 300 K to 2 K and magnetic field ranges from 0 T to 16 T.

The valence state of relevant elements after the deposition of a-LAO was investigated by a Thermo Scientific ESCALAB Xi^+ XPS, using a monochromatic Al Kα X-ray source with a photon energy of 1,486.6 eV. This leads to a kinetic energy of Ti 2*p* electrons of roughly 1,028 eV. The pass energy used for the high resolution scan was 50 eV. For analyzing the Ti $2p_{3/2}$ peaks, a Smart

background was subtracted and the spectra were normalized to the total area below the Ti peaks ([Ti]=[Ti^{4+}]+[Ti^{3+}]+[Ti^{2+}]=100%). The binding energies obtained from this work (458.6 ±0.1 eV for Ti^{4+}, 457.0 ±0.1 eV for Ti^{3+}, and 455.3 ±0.1 eV for Ti^{2+}) are in excellent agreement with the corresponding values (458.7 ±0.2 eV, 457.1 ±0.4 eV, and 455.3 ±0.4 eV) from the NIST Standard Reference Database 20, Version 4.1 (web version).

3. RESULTS

Fig. 1(a) is a schematic illustration of the heterostructure investigated here which consists of an a-LAO capping layer deposited on one of the three TiO_2-based substrates: STO, TiO_2(A) and TiO_2(R). To illustrate the intrinsic difference in the Ti-O configuration among the three substrates, the atomic structures of the three (001)-orientated substrates are also shown in Fig. 1(b)-(d). The STO substrate is a perovskite oxide with a lattice parameter of 3.905 Å, which consists of alternating uncharged SrO and TiO_2 sublayers. Its TiO_2-terminated surface has a Ti-O-Ti angle as large as 180º. The TiO_2(A) and TiO_2(R) belong to the ditetragonal dipyramidal class with different lattice parameters: a = b = 3.784 Å, c = 9.515 Å for the TiO_2(A) and a = b = 4.594 Å, c = 2.959 Å for the TiO_2(R). The Ti-O-Ti angle is 155.4º for the TiO_2(A) and 130.4º and 99.1º for the TiO_2(R). Shortly, by changing the substrate from STO to TiO_2(A) and then to TiO_2(R), we can continuously decrease the Ti-O-Ti angle, thus tune the hybridization between O_{2p} and Ti_{3d} e_g orbitals.[30]

The temperature-dependent sheet resistance (R_s), sheet carrier density (n_s) and mobility (μ) of the three heterostructures are shown in Fig. 2. The a-LAO/STO heterointerface is metallic as reported before.[18, 22] The Hall resistance, R_{xy}, is nonlinear (Fig. 3(a)) below 50 K which is probably due to the presence of two-band transport carriers (details on the two-band model are shown in the Supporting

Information S2).[31] The n_s in Fig. 2(b) is deduced from the linear part of R_{xy} in the low magnetic field in Fig. 3(a) and it is nearly constant in the temperature (T) range of 100-295 K with a value of 1.0×10^{14} cm^{-2}. As T decreases below 100 K, the n_s decreases and reaches a value around 2.2×10^{13} cm^{-2} at 2 K due to the carrier freeze-out. The μ increases upon cooling and is about 370 $cm^2V^{-1}s^{-1}$ at 2 K.

The a-LAO/TiO_2(A) heterointerface shows a metallic behavior similar to the a-LAO/STO in the temperature range125 K < T < 295 K. As the temperature decreases below 125K, the R_s for the a-LAO/TiO_2(A) displays a smooth upturn. Two possibilities account for this upturn: (1) a Kondo effect[32-33] caused by the enhanced spin scattering of charge carriers by localized magnetic moments,[34-35] or (2) a 2D weak localization effect, caused by self-interference of wave packets when they are coherently back scattered by impurities.[36] In order to distinguish between these two effects, we implement the Kondo effect model[37] as well as 2D weak localization model[38] to study what is the origin of the resistance upturn. Compared to the weak localization, the Kondo effect can better explain our R_s - T behavior, which is in contrast to the mechanism described by Sarkar *et al*.[28] The Kondo model was fitted using the following expression[37]:

$$R(T) = R_0 + \mathrm{q}T^2 + \mathrm{p}T^5 + R_{K,0}\left(\frac{1}{1+(2^{1/\mathrm{s}}-1)(T/T_\mathrm{K})^2}\right)^\mathrm{s} \quad (1)$$

where R_0 is the residual resistance due to the disorder, the T^2 and T^5 terms represent the temperature dependences of electron-electron and electron-phonon interactions, respectively. The last term in Eqs. (1) is the Kondo contribution, where $R_{K,0}$ is the Kondo resistance at zero temperature and T_K is the Kondo temperature defined as the temperature at which the Kondo resistance is half relative to its zero-temperature value. The parameter s is fixed at 0.225 according to the theoretical result obtained from the numerical renormalization group.[39-40] As shown in Fig.

3(b), the R_s was well fitted and the relative coefficients are: $R_0 = 942.6\ \Omega$, q = $7.3\times10^{-4}\ \Omega/K^2$, p = $1.3\times10^{-9}\ \Omega/K^5$, $R_{K,0} = 1202.9\ \Omega$ and $T_K = 86.2$ K. When $T << T_K$, the Kondo singlet state[41] emerges and the magnetic scattering centers are screened by charge carriers and turn nonmagnetic. This effect is manifested itself by the R_s upturn which slows down and saturates at low temperatures.[37] In contrast, for the 2D weak localization effect, the R_s upturn will never saturate (Supporting Information S3). As for the n_s of the a-LAO/TiO_2(A), it is nearly constant, $(1.3\text{-}2.1)\times10^{14}$ cm^{-2}, from 295 K to 2 K, which is comparable to that of the a-LAO/STO for $T > 125$ K. Meanwhile, the μ of a-LAO/TiO_2(A) locates at the range from 13.0 to 24.5 $cm^{-2}V^{-1}s^{-1}$ from 295 K to 2 K, much lower than that of a-LAO/STO for $T < 125$ K. The low electron mobility of the a-LAO/TiO_2(A) could be due to the Kondo scattering.

As the temperature decreases, the a-LAO/TiO_2(R) first exhibits a metallic-like behavior from 295 K to 45 K and then a metal-to-insulator transition around 45 K, due to the freeze-out of charge carriers. For $T < 20$ K, R_s becomes so large that it is well beyond the limits of our measurement system (Fig. 2(a)). Hall effect measurements are therefore only reliable in the temperature range of 30 K < T < 125 K, which display a n_s of 5.6×10^{12} cm^{-2} at 125 K and 2.5×10^{11} cm^{-2} at 30 K (Fig. 2(b)). The value of n_s for the a-LAO/TiO_2(R) is more than 2 orders of magnitude lower than the former two systems at low temperature ($T \leq 30$ K). In contrast, μ increases as temperature decreases from 125 K to 30 K and reaches a value of 77 $cm^{-2}V^{-1}s^{-1}$ at 30 K (Fig. 2(c)). It is comparable with that of a-LAO/STO, and higher than that of a-LAO/TiO_2(A). Notably, below 38 K, the R_s can be well fitted by a small polaron model[42] (Fig. 3(c)):

$$\ln\left(\frac{R_s}{T}\right) = \ln(A) + \frac{E_p}{k_B T} \quad (2)$$

where A is a temperature independent constant, E_p is the activation energy for hopping condution and k_B is the Boltzmann constant. Through fitting, the deduced activation energy is 14 meV that is comparable with Co doped TiO_2,[43] indicating that the transport proceeds through thermal activation.[44]

To reveal the physical origin of the interfacial conductivity and mechanisms that lead to the different transport properties of these three heterostructures, we further performed an analysis of the oxidization state of relevant elements by XPS. In the stoichiometric single crystalline STO and TiO_2 substrates, the valence states of the Ti cations and O anions are Ti^{4+} and O^{2-}, respectively. During the deposition of a-LAO, the O anions will diffuse out of the substrate to oxidize the reactive plasma species absorbed on the substrate surface.[18, 21] This results in the formation of oxygen vacancies. Obviously, once an oxygen vacancy forms, two electrons will be transferred to nearby Ti^{4+} cations, reducing the valence state of Ti^{4+} cations to either Ti^{3+} or Ti^{2+}. Fig. 4(a) shows the Ti 2*p* spectra in the three heterostructures. The main peaks at the binding energy of 458.6 eV correspond to Ti^{4+} cations, and the right side shoulders at the binding energy of 457 eV and 455.3 eV stem from Ti^{3+} and Ti^{2+} cations. A quantitative analysis shown in Fig. 4(b)-(d) gives the relative concentrations of Ti^{3+} and Ti^{2+} cations (Table I). It turns out, among these three heterostructures, the a-LAO/TiO_2(A) has the largest percentages of Ti^{3+} and Ti^{2+} cations, which are 17.5% and 6.5%, respectively. The a-LAO/STO has comparable percentages of Ti^{3+} and Ti^{2+} cations (15.9% and 4.7%), whereas a-LAO/TiO_2(R) shows the lowest Ti^{3+} and Ti^{2+} concentrations (5.7% and 1.8%) more than three times lower than the former two systems. Shortly, the Ti^{3+} and Ti^{2+} concentrations and thus the concentration of oxygen vacancies in the TiO_2-based substrates show a similar trend with n_s upon changing the substrates from STO to TiO_2(A), and then to TiO_2(R). Note that the carrier concentration deduced from XPS is always higher than that of n_s determined by Hall measurements. This could be due to the presence of localized carriers which

can be detected by XPS but not sensitive to Hall measurements. Based on the XPS result and the nonpolar of capping layers, we can conclude that the mobile charge carriers in the heterointerfaces mainly come from the oxygen vacancies in the substrates. It should be noted that although there are reports on that Ti interstitials contribute to the band gap states[45] or the Ti^{3+} and Ti^{2+} concentrations of TiO_2(R) surface. However, recent electron bombardment results confirm that oxygen vacancies rather than Ti interstitials make the dominant contribution to the electron reconstruction.[46]

4. DISCUSSION

The difference in transport properties of these three types of conductive heterointerfaces is related to the different concentrations of oxygen vacancies in the substrates. Since we used the same capping layer of a-LAO, therefore, the driving force underlying the redox reaction remains the same. The different content of oxygen vacancies should result from a different surface formation energy of oxygen vacancy (**the enthalpy required to form one surface oxygen vacancy**) and/or the different activation energy for the diffusion of oxygen vacancy (**the energy barrier for an oxygen vacancy migration from one position to another at the substrate surface**). According to the previous calculations as summarized in Table II, TiO_2-terminated STO substrate has the highest surface formation energy of oxygen vacancy among the three substrates, which is 5.94 eV,[47] TiO_2(A) has a medium value in the range of 4.00-4.96 eV,[48] and TiO_2(R) possesses the lowest formation energy of oxygen vacancy on its surface (3.21 eV[49]). These oxygen vacancy formation energies seem to be monotonically increasing with the increase of Ti-O-Ti angles, such as that STO has the largest Ti-O-Ti angle (180º) and also exhibits the highest oxygen vacancy formation energy. Therefore, under the same deposition condition, oxygen vacancies are easiest to be formed in TiO_2(R), then in TiO_2(A), and finally in STO. However, the a-LAO/TiO_2(R) shows the lowest carrier concentration as well as oxygen

vacancies. This indicates that the difference in the surface formation energy of oxygen vacancy plays a negligible role in the measured difference. In other words, the driving force of the a-LAO deposition can overcome all the barriers for the interface redox reaction. Instead, the less carrier/oxygen vacancy concentration of a-LAO/TiO_2(R) is more likely due to the rather large activation energy for the diffusion of oxygen vacancies at the TiO_2(R) surface, which is around 1.5 eV due to the small Ti-O-Ti bond angle. In contrast, the activation energy for the diffusion of oxygen vacancy at the surface of STO and TiO_2(A) is much smaller, which could be only 0.1-0.2 eV.[47, 50] Therefore, it is the activation dynamics of oxygen vacancies that determine the differences in the formation of 2DEGs among these three heterostructures. Since the activation energy for the diffusion of oxyen vacancies is high at the TiO_2(R) surface, the formation of oxygen vacancy is probably thermodynamically limited to the substrate surface. Compared to the other two interfaces, the oxygen ions at the TiO_2(R) surface are more difficult to diffuse outward to oxidize the reactive plasma species absorbed on the substrate surface, therefore, results in the less concentration of oxygen vacancies.

5. CONCLUSION

To conclude, we have successfully demonstrated the formation of 2DEG at the interface between a-LAO and the TiO_2(A) as well as TiO_2(R) substrates. The TiO_2(A)-based heterostructure presents a comparable carrier density to the intensively-investigated system of a-LAO/STO, but with a much lower mobility even at low temperatures due to the occurrence of Kondo effect. In contrast, the a-LAO/TiO_2(R) gives rise to a low carrier density which is more than two orders of magnitude lower than that of a-LAO/STO and a-LAO/TiO_2(A) at low temperatures. The origin of the interfacial 2DEGs is further investigated by XPS. The lower carrier density of a-LAO/TiO_2(R) is probably due to its larger activation energy for the diffusion of oxygen vacancy at the TiO_2(R) surface than the other two

heterostructures. This work demonstrates the possibility to tune the conductive oxide heterointerface by changing the chemical environment.

Supporting Information

The Supporting Information is available from the ACS Publications or from the author.

XRD data of TiO_2(A) substrate; AFM images of STO, TiO_2(A) and TiO_2(R) substrates; **Two-band model fitting for the nonlinear Hall resistance of a-LAO/STO heterointerface;** 2D weak localization fitting for the R_s of a-LAO/TiO_2(A) heterointerface; The transport information for a-LAO/STO, a-LAO/TiO_2(A) and a-LAO/TiO_2(R) with different thickness (3 nm, 16 nm) of capping layers.

AUTHOR INFORMATION

Corresponding Author:

E-mail: yunc@dtu.dk

jrsun@iphy.ac.cn*

ACKNOWLEDGEMENT

This work has been supported by the National Basis Research of China (2013CB921700, 2016YFA0300701), the National Natural Science Foundation of China (11520101002, 51590880, 11374348, 11134007, 11574376 and 11574366) and the Key Program of the Chinese Academy of Sciences.

REFERENCE:

(1) Ohtomo, A.; Hwang, H. Y.; A High-Mobility Electron Gas at the $LaAlO_3/SrTiO_3$ Heterointerface. *Nature* **2004**, *427*, 423-426.

(2) Chen, Y. Z.; Trier, F.; Kasama, T.; Christensen, D. V.; Bovet, N.; Balogh, Z. I.; Li, H.; Thyden, K. T.; Zhang, W.; Yazdi, S.; Norby, P.; Pryds, N.; Linderoth, S.; Creation of High Mobility Two-Dimensional Electron Gases via Strain Induced Polarization at an otherwise Nonpolar Complex Oxide Interface. *Nano Lett.* **2015**, *15*, 1849-1854.

(3) Perna, P.; Maccariello, D.; Radovic, M.; Scotti di Uccio, U.; Pallecchi, I.; Codda, M.; Marré, D.; Cantoni, C.; Gazquez, J.; Varela, M.; Pennycook, S. J.; Granozio, F. M.; Conducting Interfaces between Band Insulating Oxides: The $LaGaO_3/SrTiO_3$ Heterostructure. *Appl. Phys. Lett.* **2010**, *97*, 152111.

(4) Chen, Y. Z.; Bovet, N.; Trier, F.; Christensen, D. V.; Qu, F. M.; Andersen, N. H.; Kasama, T.; Zhang, W.; Giraud, R.; Dufouleur, J.; Jespersen, T. S.; Sun, J. R.; Smith, A.; Nygard, J.; Lu, L.; Buchner, B.; Shen, B. G.; Linderoth, S.; Pryds, N.; A High-Mobility Two-Dimensional Electron Gas at the Spinel/Perovskite Interface of Gamma-$Al_2O_3/SrTiO_3$. *Nat. Commun.* **2013**, *4*, 1371.

(5) Reyren, N.; Thiel, S.; Caviglia, A. D.; Kourkoutis, L. F.; Hammerl, G.; Richter, C.; Schneider, C. W.; Kopp, T.; Rüetschi, A. S.; Jaccard, D.; Gabay, M.; Muller, D. A.; Triscone, J. M.; Mannhart, J.; Superconducting Interfaces Between Insulating Oxides. *Science* **2007**, *317*, 1196-1199.

(6) Brinkman, A.; Huijben, M.; van Zalk, M.; Huijben, J.; Zeitler, U.; Maan, J. C.; van der Wiel, W. G.; Rijnders, G.; Blank, D. H.; Hilgenkamp, H.; Magnetic Effects at the Interface Between Non-Magnetic Oxides. *Nat. Mater.* **2007**, *6*, 493-496.

(7) Lin, W. N.; Ding, J. F.; Wu, S. X.; Li, Y. F.; Lourembam, J.; Shannigrahi, S.; Wang, S. J.; Wu, T.; Electrostatic Modulation of $LaAlO_3/SrTiO_3$ Interface Transport in an Electric Double-Layer Transistor. *Adv. Mater. Interfaces* **2014**, *1*, 1300001.

(8) Lei, Y.; Li, Y.; Chen, Y. Z.; Xie, Y. W.; Chen, Y. S.; Wang, S. H.; Wang, J.; Shen, B. G.; Pryds, N.; Hwang, H. Y.; Sun, J. R.; Visible-Light-Enhanced Gating Effect at the $LaAlO_3/SrTiO_3$ Interface. *Nat. Commun.* **2014**, *5*, 5554.

(9) Chen, Y. Z.; Green, R. J.; Sutarto, R.; He, F. Z.; Linderoth, S.; Sawatzky, G. A.; Pryds, N.; Tuning the Two-Dimensional Electron Liquid at Oxide Interfaces by Buffer-Layer-Engineered Redox Reactions. *Nano Lett.* **2017**, *17*, 7062–7066.

(10) Chen, Y. Z.; Trier, F.; Wijnands, T.; Green, R. J.; Gauquelin, N.; Egoavil, R.; Christensen, D. V.; Koster, G.; Huijben, M.; Bovet, N.; Macke, S.; He, F.; Sutarto, R.; Andersen, N. H.; Sulpizio, J. A.; Honig, M.; Prawiroatmodjo, G. E.; Jespersen, T. S.; Linderoth, S.; Ilani, S.; Verbeeck, J.; Van Tendeloo, G.; Rijnders, G.; Sawatzky, G. A.; Pryds, N.; Extreme Mobility Enhancement of Two-Dimensional Electron Gases at Oxide Interfaces by Charge-Transfer-Induced Modulation Doping. *Nat. Mater.* **2015**, *14*, 801-806.

(11) Wu, S.; Luo, X.; Turner, S.; Peng, H.; Lin, W.; Ding, J.; David, A.; Wang, B.; Van Tendeloo, G.; Wang, J.; Wu, T.; Nonvolatile Resistive Switching in $Pt/LaAlO_3/SrTiO_3$ Heterostructures. *Phys. Rev. X* **2013**, *3*, 041027.

(12) Nakagawa, N.; Hwang, H. Y.; Muller, D. A.; Why Some Interfaces Cannot be Sharp. *Nat. Mater.* **2006**, *5*, 204-209.

(13) Siemons, W.; Koster, G.; Yamamoto, H.; Harrison, W. A.; Lucovsky, G.; Geballe, T. H.; Blank, D. H.; Beasley, M. R.; Origin of Charge Density at $LaAlO_3$ on $SrTiO_3$ Heterointerfaces: Possibility of Intrinsic Doping. *Phys. Rev. Lett.* **2007**, *98*, 196802.

(14) Herranz, G.; Basletic, M.; Bibes, M.; Carretero, C.; Tafra, E.; Jacquet, E.; Bouzehouane, K.; Deranlot, C.; Hamzic, A.; Broto, J. M.; Barthelemy, A.; Fert, A.; High Mobility in $LaAlO_3/SrTiO_3$ Heterostructures: Origin, Dimensionality, and Perspectives. *Phys. Rev. Lett.* **2007**, *98*, 216803.

(15) Kalabukhov, A.; Gunnarsson, R.; Börjesson, J.; Olsson, E.; Claeson, T.; Winkler, D.; Effect of Oxygen Vacancies in the $SrTiO_3$ Substrate on the Electrical Properties of the $LaAlO_3$ ／ $SrTiO_3$ Interface. *Phys. Rev. B* **2007**, *75*, 121404.

(16) Chambers, S. A.; Engelhard, M. H.; Shutthanandan, V.; Zhu, Z.; Droubay, T. C.; Qiao, L.; Sushko, P. V.; Feng, T.; Lee, H. D.; Gustafsson, T.; Garfunkel, E.; Shah, A. B.; Zuo, J. M.; Ramasse, Q. M.; Instability, Intermixing and Electronic Structure at the Epitaxial $LaAlO_3/SrTiO_3(001)$ Heterojunction. *Surf. Sci. Rep.* **2010**, *65*, 317-352.

(17) Gunkel, F.; Hoffmann-Eifert, S.; Heinen, R. A.; Christensen, D. V.; Chen, Y. Z.; Pryds, N.; Waser, R.; Dittmann, R.; Thermodynamic Ground States of Complex Oxide Heterointerfaces. *ACS Appl. Mater. Interfaces* **2017**, *9*, 1086-1092.

(18) Chen, Y. Z.; Pryds, N.; Kleibeuker, J. E.; Koster, G.; Sun, J.; Stamate, E.; Shen, B.; Rijnders, G.; Linderoth, S.; Metallic and Insulating Interfaces of Amorphous $SrTiO_3$-based Oxide Heterostructures. *Nano Lett.* **2011**, *11*, 3774-3778.

(19) Chen, Y. Z.; Bovet, N.; Kasama, T.; Gao, W. W.; Yazdi, S.; Ma, C.; Pryds, N.; Linderoth, S.; Room Temperature Formation of High-Mobility Two-Dimensional Electron Gases at Crystalline Complex Oxide Interfaces. *Adv. Mater.* **2014**, *26*, 1462-1467.

(20) Shibuya, K.; Ohnishi, T.; Lippmaa, M.; Oshima, M.; Metallic Conductivity at the $CaHfO_3$ / $SrTiO_3$ Interface. *Appl. Phys. Lett.* **2007**, *91*, 232106.

(21) Posadas, A. B.; Kormondy, K. J.; Guo, W.; Ponath, P.; Geler-Kremer, J.; Hadamek, T.; Demkov, A. A.; Scavenging of Oxygen from $SrTiO_3$ During Oxide Thin Film Deposition and the Formation of Interfacial 2DEGs. *J. Appl. Phys.* **2017**, *121*, 105302.

(22) Chen, Y. Z.; Christensen, D. V.; Trier, F.; Pryds, N.; Smith, A.; Linderoth, S.; On the Origin of Metallic Conductivity at the Interface of $LaAlO_3/SrTiO_3$. *Appl. Surf. Sci.* **2012**, *258*, 9242-9245.

(23) Lee, S. W.; Liu, Y.; Heo, J.; Gordon, R. G.; Creation and Control of Two-Dimensional Electron Gas Using Al-Based Amorphous Oxides/$SrTiO_3$ Heterostructures Grown by Atomic Layer Deposition. *Nano Lett.* **2012**, *12*, 4775-4783.

(24) Rodel, T. C.; Fortuna, F.; Sengupta, S.; Frantzeskakis, E.; Le Fevre, P.; Bertran, F.; Mercey, B.; Matzen, S.; Agnus, G.; Maroutian, T.; Lecoeur, P.; Santander-Syro, A. F.; Universal Fabrication of 2D Electron Systems in Functional Oxides. *Adv. Mater.* **2016**, *28*, 1976-1980.

(25) Chen, Y. Z.; Döbeli, M.; Pomjakushina, E.; Gan, Y. L.; Pryds, N.; Lippert, T.; Scavenging of Oxygen Vacancies at Modulation-Doped Oxide Interfaces: Evidence from Oxygen Isotope Tracing. *Phys. Rev. Mater.* **2017**, *1*, 052002.

(26) Schneider, C. W.; Esposito, M.; Marozau, I.; Conder, K.; Doebeli, M.; Hu, Y.; Mallepell, M.; Wokaun, A.; Lippert, T.; The Origin of Oxygen in Oxide Thin Films: Role of the Substrate. *Appl. Phys. Lett.* **2010**, *97*, 192107.

(27) Scigaj, M.; Gázquez, J.; Varela, M.; Fontcuberta, J.; Herranz, G.; Sánchez, F.; Conducting Interfaces Between Amorphous Oxide Layers and $SrTiO_3$ (110) and $SrTiO_3$ (111). *Solid State Ionics* **2015**, *281*, 68-72.

(28) Sarkar, T.; Gopinadhan, K.; Zhou, J.; Saha, S.; Coey, J. M.; Feng, Y. P.; Ariando; Venkatesan, T.; Electron Transport at the TiO_2 Surfaces of Rutile, Anatase, and Strontium Titanate: The Influence of Orbital Corrugation. *ACS Appl. Mater. Interfaces* **2015**, *7*, 24616-24621.

(29) Cheng, J.; Luo, J.; Yang, K.; Comparison Studies of Interfacial Electronic and Energetic Properties of $LaAlO_3/TiO_2$ and $TiO_2/LaAlO_3$ Heterostructures from First-Principles Calculations. *ACS Appl. Mater. Interfaces* **2017**, *9*, 7682-7690.

(30) Lechermann, F.; Heckel, W.; Kristanovski, O.; Müller, S.; Oxygen-Vacancy Driven Electron Localization and Itinerancy in Rutile-Based TiO_2. *Phys. Rev. B* **2017**, *95*, 195159.

(31) Kim, J. S.; Seo, S. S. A.; Chisholm, M. F.; Kremer, R. K.; Habermeier, H. U.; Keimer, B.; Lee, H. N.; Nonlinear Hall Effect and Multichannel Conduction in $LaTiO_3/SrTiO_3$ Superlattices. *Phys. Rev. B* **2010**, *82*, 201407.

(32) Zhang, S.; Ogale, S. B.; Yu, W.; Gao, X.; Liu, T.; Ghosh, S.; Das, G. P.; Wee, A. T. S.; Greene, R. L.; Venkatesan, T.; Electronic Manifestation of Cation-Vacancy-Induced Magnetic Moments in a Transparent Oxide Semiconductor: Anatase Nb:TiO_2. *Adv. Mater.* **2009**, *21*, 2282-2287.

(33) Jun, K.; Resistance Minimum in Dilute Magnetic Alloys. *Progr. Theor. Phys.* **1964**, *32*, 37-49.

(34) Li, Y.; Deng, R.; Lin, W.; Tian, Y.; Peng, H.; Yi, J.; Yao, B.; Wu, T.; Electrostatic Tuning of Kondo Effect in a Rare-Earth-Doped Wide-Band-Gap Oxide. *Phys. Rev. B* **2013**, *87*, 155151.

(35) Yan, H.; Zhang, Z.; Wang, S.; Zhang, H.; Chen, C. L.; Jin, K.; Modulated Transport Behavior of Two-Dimensional Electron Gas at Ni-Doped $LaAlO_3$/$SrTiO_3$ Heterointerfaces. *ACS Appl. Mater. Interfaces* **2017**, *9*, 39011-39017.

(36) Lee, P. A.; Ramakrishnan, T. V.; Disordered Electronic Systems. *Rev. Mod. Phys.* **1985**, *57*, 287-337.

(37) Lee, M.; Williams, J. R.; Zhang, S.; Frisbie, C. D.; Goldhaber-Gordon, D.; Electrolyte Gate-Controlled Kondo Effect in $SrTiO_3$. *Phys. Rev. Lett.* **2011**, *107*, 256601.

(38) Niu, W.; Gao, M.; Wang, X.; Song, F.; Du, J.; Wang, X.; Xu, Y.; Zhang, R.; Evidence of Weak Localization in Quantum Interference Effects Observed in Epitaxial $La_{0.7}Sr_{0.3}MnO_3$ Ultrathin Films. *Sci. Rep.* **2016**, *6*, 26081.

(39) T. A. Costi; A. C. Hewson; Zlatic, V.; Transport Coefficients of the Anderson Model via the Numerical Renormalization Group. *J. Phys.: Condens. Matter* **1994**, *6*, 2519-2558.

(40) Goldhaber-Gordon, D.; Gores, J.; Kastner, M. A.; From the Kondo Regime to the Mixed-Valence Regime in a Single-Electron Transistor. *Phys. Rev. Lett.* **1998**, *81*, 5225-5228.

(41) Zhang, G.; Gu, Q.; Kondo Spin Liquid and Magnetically Long-Range Ordered States in the Kondo Necklace Model. *Phys. Rev. B* **2000**, *62*, 69-72.

(42) Khan, W.; Naqvi, A. H.; Gupta, M.; Husain, S.; Kumar, R.; Small Polaron Hopping Conduction Mechanism in Fe Doped $LaMnO_3$. *J. Chem. Phys.* **2011**, *135*, 054501.

(43) Jaćimović, J.; Horváth, E.; Náfrádi, B.; Gaál, R.; Nikseresht, N.; Berger, H.; Forró, L.; Magrez, A.; From Nanotubes to Single Crystals: Co doped TiO_2. *APL Mater.* **2013**, *1*, 032111.

(44) Yildiz, A.; Lisesivdin, S. B.; Kasap, M.; Mardare, D.; Non-adiabatic Small Polaron Hopping Conduction in Nb-Doped TiO_2 Thin Film. *Physica B: Condensed Matter* **2009**, *404*, 1423-1426.

(45) Wendt, S.; Sprunger, P. T.; Lira, E.; Madsen, G. K. H.; Li, Z. S.; Hansen, J. Ø.; Matthiesen, J.; Blekinge-Rasmussen, A.; Lægsgaard, E.; Hammer, B.; Besenbacher, F.; The Role of Interstitial Sites in the Ti3d Defect State in the Band Gap of Titania. *Science* **2008**, *320*, 1755-1759.

(46) Yim, C. M.; Pang, C. L.; Thornton, G.; Oxygen Vacancy Origin of the Surface Band-Gap State of TiO_2 (110). *Phys. Rev. Lett.* **2010**, *104*, 036806.

(47) Carrasco, J.; Illas, F.; Lopez, N.; Kotomin, E. A.; Zhukovskii, Y. F.; Evarestov, R. A.; Mastrikov, Y. A.; Piskunov, S.; Maier, J.; First-Principles Calculations of the Atomic and Electronic Structure of F Centers in the Bulk and on the (001) Surface of $SrTiO_3$. *Phys. Rev. B* **2006**, *73*, 064106.

(48) Linh, N. H.; Nguyen, T. Q.; Diño, W. A.; Kasai, H.; Effect of Oxygen Vacancy on the Adsorption of O_2 on Anatase TiO_2 (001): A DFT-Based Study. *Surf. Sci.* **2015**, *633*, 38-45.

(49) Benjamin, J. M.; Graeme, W. W.; A Density Functional Theory + U Study of Oxygen Vacancy Formation at the (110), (100), (101), and (001) Surfaces of Rutile TiO_2. *J. Phys. Chem. C* **2009**, *113*, 7322-7328.

(50) Uberuaga, B. P.; Bai, X. M.; Defects in Rutile and Anatase Polymorphs of TiO2: Kinetics and Thermodynamics near Grain Boundaries. *J. Phys: Condens. Matter.* **2011**, *23*, 435004.

Figures and Figure captions:

FIG. 1 (a) A schematic illustration of the oxide heterostructure, consisting of an amorphous $LaAlO_3$ (a-LAO) capping layer and a TiO_2-based substrate. The unit cell lattice and the Ti-O configuration (Ti-O-Ti bond angle) of the three types of substrates: (b) $SrTiO_3$ (STO), (c) anatase TiO_2 [TiO_2(A)] and (d) rutile TiO_2 [TiO_2(R)].

FIG. 2 Temperature dependence of (a) sheet resistance, R_s, (b) carrier density, n_s, and (c) electron Hall mobility, μ, of 2DEGs created at the interface between the capping layer of a-LAO and the substrate of TiO_2-terminated STO (blue circles), TiO_2(A) (green squares) and TiO_2(R) (purple triangles), respectively.

FIG. 3 (a) Magnetic field dependence of the Hall resistance (R_{xy}) for the a-LAO/STO interface, measured in the temperature from 295 K to 2 K. (b) Temperature-dependent R_s of the a-LAO/TiO_2(A) (green dots) is fitted by Kondo effect (black line). (c) Temperature-dependent ln (R_s/T) of the a-LAO/TiO_2(R) (purple dots) is fitted by small polaron model (black line).

FIG. 4 (a) The Ti 2*p* X-ray photoelectron spectroscopy (XPS) of a-LAO/STO, a-LAO/TiO_2(A) and a-LAO/TiO_2(R). (b)-(d) Fitting of the XPS intensity signals of these three heterostructures. The measurements are performed at room temperature.

FIG. 1

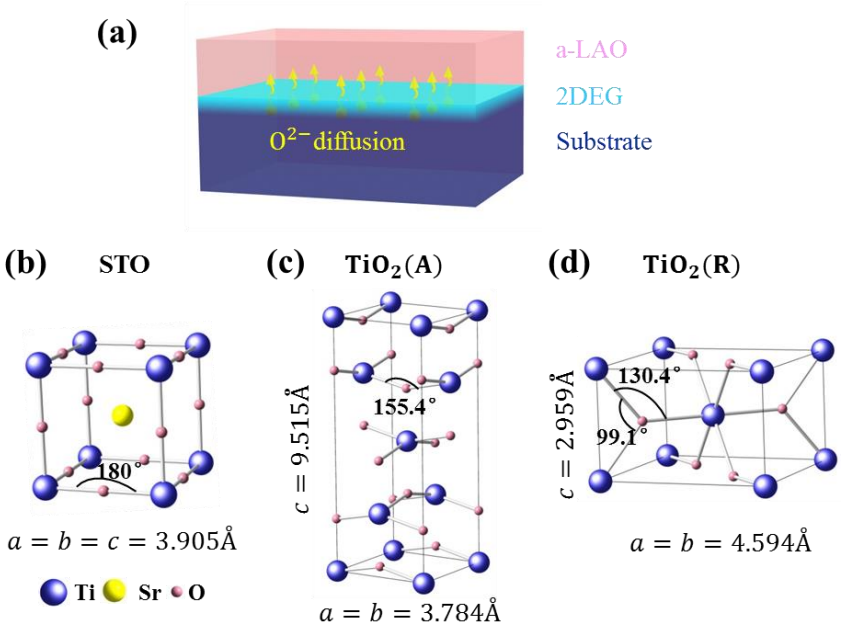
(a)
a-LAO
2DEG
Substrate
O^{2-} diffusion
(b) STO
180°
$a = b = c = 3.905$Å
Ti
Sr
O
(c) TiO_2(A)
155.4°
$c = 9.515$Å
$a = b = 3.784$Å
(d) TiO_2(R)
130.4°
99.1°
$c = 2.959$Å
$a = b = 4.594$Å

FIG. 2

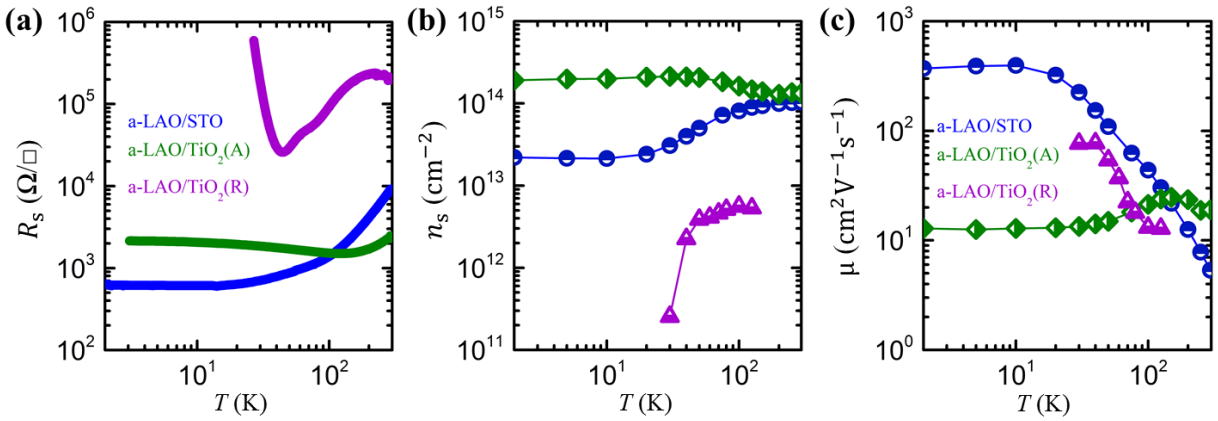
(a)
(b)
(c)
a-LAO/STO
a-LAO/TiO2(A)
a-LAO/TiO2(R)
Rs (Ω/□)
ns (cm−2)
μ (cm2V−1s−1)
T (K)
T (K)
T (K)

FIG. 3

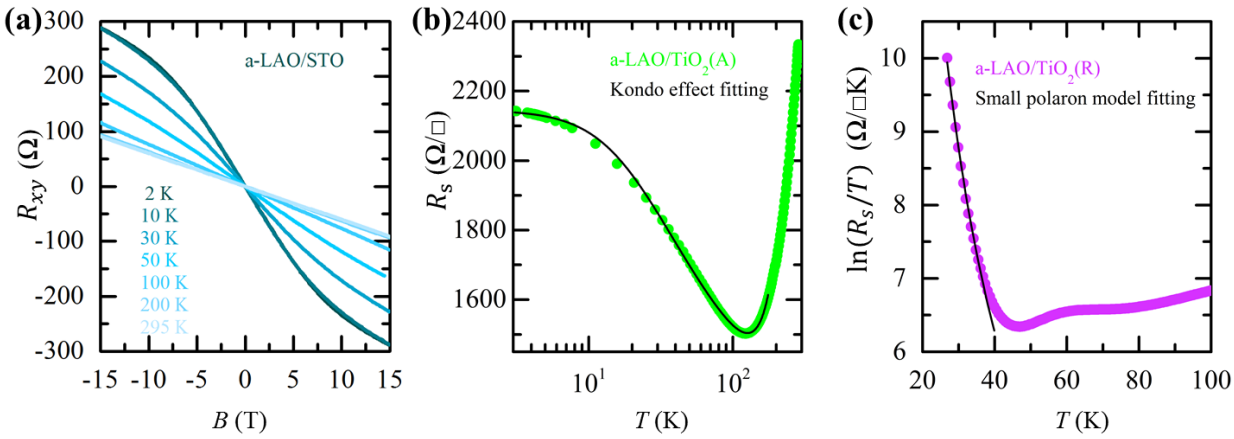
(a)
a-LAO/STO
2 K
10 K
30 K
50 K
100 K
200 K
295 K
R_{xy} (Ω)
B (T)
(b)
a-LAO/TiO$_2$(A)
Kondo effect fitting
R_S (Ω/□)
T (K)
(c)
a-LAO/TiO$_2$(R)
Small polaron model fitting
$\ln(R_S/T)$ (Ω/□K)
T (K)

FIG. 4

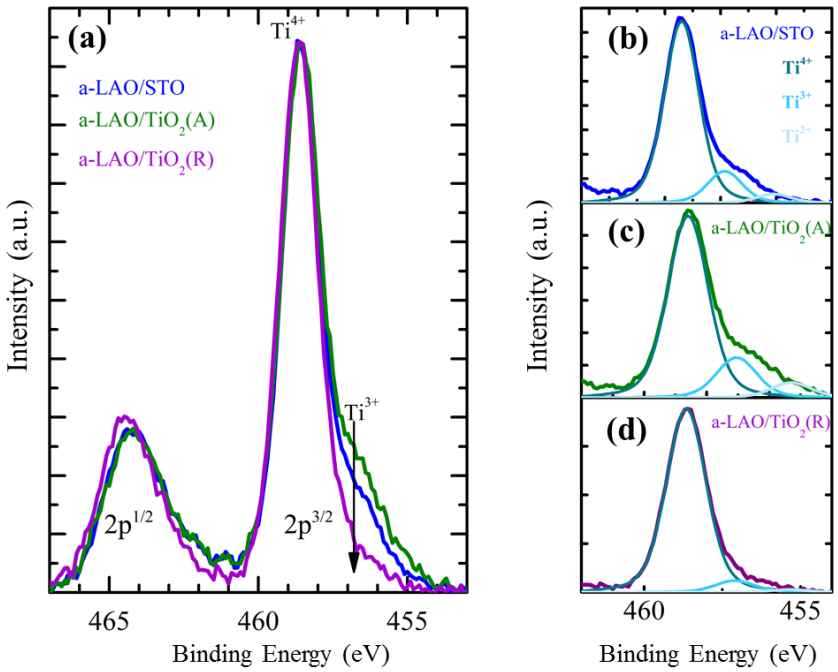
(a)
Ti4+
a-LAO/STO
a-LAO/TiO2(A)
a-LAO/TiO2(R)
Ti3+
2p1/2
2p3/2
Intensity (a.u.)
465
460
455
Binding Energy (eV)
(b)
a-LAO/STO
Ti4+
Ti3+
Ti2+
(c)
a-LAO/TiO2(A)
(d)
a-LAO/TiO2(R)
Intensity (a.u.)
460
455
Binding Energy (eV)

Table I. The amounts of cations determined by XPS measurements and the Hall carrier densities at 295 K in the three heterointerfaces:

	Ti^{4+} (%)	Ti^{3+} (%)	Ti^{2+} (%)	n_s (cm^{-2})
a-LAO/STO	79.4	15.9	4.7	1.0×10^{14}
a-LAO/TiO_2(A)	76.0	17.5	6.5	1.3×10^{14}
a-LAO/TiO_2(R)	92.5	5.7	1.8	5.6×10^{12}

Table II. The formation energy of an oxygen vacancy and the activation energy for the diffusion of oxygen vacancy on the surface of STO, TiO_2(A) and TiO_2(R):

	STO	TiO_2(A)	TiO_2(R)
Formation energy (eV)	5.94[47]	4.00-4.96[48]	3.21[49]
Activation energy (eV)	0.1-0.2[47]	0.2[50]	1.5[50]

Table of Contents Graphic